Journal of Materials and Environmental Science
ISSN : 2028-2508
e-ISSN : 2737-890X
CODEN : JMESCN

J. Mater. Environ. Sci., 2026, Volume 17, Issue 7, Page 1117-1138

http://www.jmaterenvironsci.com

Inhibition Behaviour of Low Carbon Steel by Synthesized and Characterized Calcium Oxide/Silica Nanocomposite In 15% HCl and 15% H_2SO_4 Solution

Kufre E. E.*, Akanimo N. E., Aniedi E. N.

Department of Chemistry, Research Unit, Akwa Ibom State University, P.M.B. 1167, Nigeria

**Corresponding author, Email address: kufreessien@aksu.edu.ng*

SPONSORED BY: Tertiary Education Trust Fund, Nigeria

Received *04 June 2026,*
Revised *05 July 2026,*
Accepted *06 July 2026*

Keywords:
- ✓ *Nanocomposite;*
- ✓ *corrosion;*
- ✓ *low-carbon steel;*
- ✓ *Langmuir adsorption;*
- ✓ *Adsorption*

Citation*: Kufre E. E., Akanimo N. E., Aniedi E. N. (2026) Inhibition Behaviour of Low Carbon Steel by Synthesized and Characterized Calcium Oxide/Silica Nanocomposite In 15% HCl and 15% H_2SO_4 Solution, J. Mater. Environ. Sci., 17(7), 1117-1138.*

Abstract: The corrosion protection capability of a synthesized CaO/SiO_2 nanocomposite for low-carbon steel in 15% HCl and 15% H_2SO_4 solutions was investigated using weight loss measurements, Langmuir adsorption, potentiodynamic polarization, electrochemical impedance spectroscopy (EIS), SEM/EDX, and XRD techniques. Weight loss results revealed that inhibition efficiency increased with inhibitor concentration but decreased with temperature, reaching maximum values of 94% in HCl and 86% in H_2SO_4 at 303 K. Adsorption followed the Langmuir isotherm (R^2 = 0.978–0.995), while negative values of $\Delta G°$, $\Delta H°$, and $\Delta S°$ indicated a spontaneous, exothermic adsorption process dominated by physisorption. Polarization and EIS analyses revealed that the CaO/SiO_2 nanocomposite acted as a mixed-type inhibitor by increasing charge-transfer resistance and suppressing both anodic and cathodic reactions through the formation of a protective barrier film. SEM micrographs revealed reduced surface deterioration and pitting in the protected samples, whereas EDX detected the presence of Ca, Si, and O on the steel surface, confirming the adsorption of the nanocomposite. XRD analysis revealed suppression of crystalline corrosion products and the formation of an amorphous protective CaO/SiO_2 layer. Overall, the synthesized CaO/SiO_2 nanocomposite provided effective corrosion protection in both acidic media, with superior performance in HCl, demonstrating its potential as an efficient and environmentally friendly corrosion inhibitor for acidic industrial applications.

1. Introduction

The excellent mechanical strength, ductility, availability, and relatively low cost of iron and low-carbon steel are the primary attributes that account for their widespread use in industrial, engineering, marine, and petrochemical applications (Cunat, 2004; Bhadeshia & Honeycombe, 2024; Gao *et al.,* 2025; Jackson *et al.,* 2019). Even with these advantages, their most important challenge is vulnerability to corrosion in aggressive environments particularly in acidic media commonly used in industrial cleaning, pickling, and descaling operations (Chaudhary *et al.,* 2026; Zehra *et al.,* 2025). Corrosion considerably reduces the service life and structural integrity of metallic materials, leading to vast economic losses and safety risks worldwide (Kania, 2023).

It has been reported that corrosion inflicts substantial economic costs, accounting for a major proportion of the gross domestic product (GDP) of many national economies worldwide (Prasad *et al*., 2020; Kania, 2023; Koch *et al*., 2005; Boekom *et al*., 2020). For instance, researches have shown that corrosion damage and prevention strategies in the United States alone incurs hundreds of billions of

dollars annually, with a major portion attributed to industrial equipment failure and maintenance (Koch *et al.,* 2005; Revie & Uhlig, 2025; Essiene *et al.,* 2021). The corrosion-induced failures in pipelines and storage systems in the oil and gas sector have resulted in catastrophic incidents, environmental pollution, and loss of life, highlighting the urgent need for effective corrosion protection strategies (Vakili *et al.,* 2024; Assad *et al.,* 2025; Jackson *et al.,* 2016).

Corrosion of low carbon steel in acidic environments, such as hydrochloric acid (HCl) and sulfuric acid (H_2SO_4) proceeds predominantly through electrochemical redox reactions involving anodic metal dissolution and cathodic hydrogen evolution (Avdeev & Kuznetsov, 2022; Okolo *et al.,* 2026; BoEKOM *et al.,* 2019; Jackson *et al.,* 2016). The use of corrosion inhibitors has been commonly acknowledged as one of the most effective and economical approaches to mitigate these processes. These inhibitors operate by forming a protective barrier that minimizes direct contact between the metal and the corrosive medium (Aljibori *et al.,* 2023; Essien *et al.,* 2024b; Rauța *et al.,* 2025; Guendouz *et al.,* 2025).

Nanostructured materials are considered more effective than conventional organic inhibitors in recent times due to their high surface area, enhanced reactivity, and improved adsorption capabilities. Nanocomposites, in particular, have exhibited superior effectiveness in corrosion mitigation owing to their synergistic properties arising from their constituent phases (Muresan, 2023). Among these, calcium oxide (CaO)-based materials have attracted considerable attention owing to their strong basicity, chemical stability, and ability to form protective layers on metallic surfaces. Likewise, silica (SiO_2) is characterized by a high surface area, chemical inertness, and excellent adsorption properties. The integration of CaO and SiO_2 into a nanocomposite system is anticipated to enhance corrosion inhibition performance through synergistic interactions that promote improved surface coverage and greater stability of the protective film.

Previous studies have shown that inorganic and hybrid nanomaterials can effectively retard corrosion of steel in acidic environments by forming stable adsorption layers and limiting charge-transfer at the metal–solution interface (Lrhoul *et al.,* 2023; Gaber *et al.,* 2025; Hu & Cheng, 2025; Sasikumar *et al.,* 2025; Kufre *et al.,* 2025; Anadebe *et al.,* 2026). However, relatively few studies have investigated the combined effect of CaO/SiO_2 nanocomposites in highly aggressive dual-acid systems such as 15% HCl and 15% H_2SO_4, which are commonly encountered in industrial processes.

In this study, a synthesized and characterized calcium oxide/silica (CaO/SiO_2) nanocomposite is studied as a corrosion inhibitor for low carbon steel in 15% HCl and 15% H_2SO_4 solutions. The study aims to determine its inhibition efficiency using gravimetric and electrochemical considerations, and to elucidate the adsorption mechanism governing corrosion protection. The effect of concentration, immersion time, and acid medium on the corrosion behavior will also be determined. Furthermore, the synergistic relationship between CaO and SiO_2 in improving surface protection is interpreted in terms of its structural and physicochemical properties. This work is anticipated to offer important understanding on environmentally friendly and high-performance nanocomposite-based corrosion inhibitors for industrial acid environments, with a view to advancing material durability and reduced economic losses due to corrosion.

2. Methodology

2.1 Gravimetric Experiments

The gravimetric (weight loss) method was used to determine the corrosion inhibition performance of the synthesized and characterized calcium oxide/silica (CaO/SiO_2) nanocomposite on low-carbon steel in 15% HCl and 15% H_2SO_4 solutions. Low-carbon steel coupons of dimensions 5.0

× 4.0 cm were mechanically polished using silicon carbide (SiC) abrasive papers of 320, 400, and 600 grit in sequence to achieve a smooth and uniform surface. The coupons were then cleaned in absolute ethanol, rinsed with distilled water, dried in acetone, and stored in moisture-free desiccators prior to use to prevent atmospheric corrosion (Oguzie *et al.,* 2013; Muazu *et al.,* 2022; Essien *et al.,* 2022; Essien *et al.,* 2024a). Different concentrations of the CaO/SiO_2 nanocomposite (typically in the range of 2.0 mg/L to 10 mg/L) were prepared by appropriate dilution of a stock suspension using distilled water. The test solutions containing 15% HCl and 15% H_2SO_4 were formulated separately, and solutions without the nanocomposite were used as blank (control) experiments.

The pre-weighed steel coupons were immersed in 100 mL of the test solutions placed in beakers and kept at temperatures ranging from 303 K to 333 K under controlled conditions. The immersion tests lasted for 10 hours, with samples withdrawn at 2-hour intervals to track corrosion progression over time. At the end of each immersion time, the coupons were carefully withdrawn from the corrosive media, rinsed with distilled water to eliminate loosely adhered corrosion products and inhibitor residues, gently scrubbed with a bristle brush, dried with acetone, and re-weighed using an analytical balance. The weight loss was calculated as the difference between the initial and final masses of the coupons at each time interval. The corrosion rate and inhibition efficiency of the CaO/SiO_2 nanocomposite were subsequently derived from the measured weight loss values in both acidic media to evaluate its protective performance on low carbon steel under varying conditions.

2.2 Potentiodynamic Polarization Measurement

The potentiodynamic polarization measurements were performed to examine the electrochemical corrosion behavior of low carbon steel in 15% HCl and 15% H_2SO_4 solutions in the absence and presence of the synthesized calcium oxide/silica (CaO/SiO_2) nanocomposite. The working electrode (low carbon steel) was introduced into the test solution and left to equilibrate for 30 minutes until a stable open circuit potential (E_oc_p) was achieved (Stefanoni *et al.,* 2015; Ozoemena *et al.,* 2023). After stabilization, polarization measurements were conducted under potentiodynamic conditions using a computer-controlled electrochemical workstation in an aerated environment. The potential was scanned at a scan rate of 1 mV s^{-1} within a potential range of −0.25 V to +0.25 V with respect to the open circuit potential. All potentials were measured against a saturated calomel electrode (SCE) as the reference electrode (Oueslati *et al.,* 2025; Obot *et al.,* 2021). The corrosion current density (i_{corr}) was derived by linear extrapolation of the anodic and cathodic Tafel regions to the corrosion potential (E_{corr}). The inhibition efficiency (η%) of the CaO/SiO_2 nanocomposite was determined using the relationship (Gopal *et al.,* 2026):

$$\eta(\%) = \frac{i^0_{corr} - i_{corr}}{i^0_{corr}} \times 100$$

where i^o_{corr} and i_{corr} represent the corrosion current densities in the absence and presence of the nanocomposite, respectively.

2.3 Electrochemical Impedance Spectroscopy (EIS) Measurement

Electrochemical impedance spectroscopy (EIS) measurements were carried out to further evaluate the corrosion inhibition performance of the CaO/SiO_2 nanocomposite on low carbon steel in 15% HCl and 15% H_2SO_4 solutions at 303 K. The experiments were performed at the open circuit potential using a small amplitude alternating current signal of 5 mV (RMS) over a frequency range of

10 Hz to 100,000 Hz under aerated conditions (Rios *et al*., 2013; Essien *et al*., 2023; Ozoemena *et al*., 2024). The impedance data were assessed using Nyquist plots, where the polarization resistance (R_p) was derived from the diameter of the semicircular capacitive loop (Wang *et al*., 2026). The polarization resistance is related to contributions from charge transfer resistance (R_{ct}), film resistance (R_f), adsorption layer resistance (Ra), and diffusion-related processes at the metal/solution interface. The inhibition efficiency (η%) was determined from the polarization resistance values using the expression:

$$\eta(\%) = \frac{R_{p(inh)} - R_p}{R_{p(inh)}} \times 100$$

where $R_{p(inh)}$ and R_p are the polarization resistance values in the presence and absence of the CaO/SiO_2 nanocomposite, respectively.

The double layer capacitance (C_{dl}) was calculated using the standard relation:

$$C_{dl} = \frac{1}{2\pi f_{max} R_p}$$

where f_{max} is the frequency at which the imaginary part of the impedance reaches its maximum value.

These electrochemical techniques collectively provide insight into the adsorption behavior, protective film formation, and charge transfer resistance enhancement induced by the CaO/SiO_2 nanocomposite on low carbon steel surfaces in aggressive acidic media.

3. Results and Discussion

3.1 Weight Loss Studies

The corrosion inhibition behaviour of the synthesized CaO/SiO_2 nanocomposite on low carbon steel in 15% H_2SO_4 and 15% HCl solutions was obtained through corrosion rate (CR), surface coverage (θ), and inhibition efficiency (IE%). The results presented in Table 1 demonstrated that the CaO/SiO_2 nanocomposite exhibited excellent protective properties, with its performance depending on inhibitor concentration, temperature, and the nature of the acidic environment. Without the inhibitor, the corrosion rate of low-carbon steel rose markedly with increasing temperature in both acidic media. This observation is consistent with the findings of Cruz-Borbolla *et al.* (2017), who reported a similar increase in the corrosion rate of steel with rising temperature in acidic media. In 15% H_2SO_4 solution, the corrosion rate increased from 4.90 $\times 10^{-3}$ mg cm^{-2} h^{-1} at 303 K to 12.30 $\times 10^{-3}$ mg cm^{-2} h^{-1} at 333 K, while in 15% HCl solution, the corrosion rate increased from 5.50 $\times 10^{-3}$ mg cm^{-2} h^{-1} to 13.50 $\times 10^{-3}$ mg cm^{-2} h^{-1}. This increase results from improved electrochemical activity at higher temperatures, which accelerates both anodic iron dissolution and cathodic hydrogen evolution reactions (Jiang & Liu, 2022).

The addition of CaO/SiO_2 nanocomposite significantly lowered the corrosion rate and improved inhibition efficiency in both acidic media. In 15% H_2SO_4, the corrosion rate decreased from 2.85 $\times 10^{-3}$ mg cm^{-2} h^{-1} at 2 mg/L inhibitor concentration to 0.65 $\times 10^{-3}$ mg cm^{-2} h^{-1} at 10 mg/L, corresponding to an increase in inhibition efficiency from 42% to 86% at 303 K. Similarly, in 15% HCl medium, the corrosion rate declined from 2.20 $\times 10^{-3}$ mg cm^{-2} h^{-1} to 0.35 $\times 10^{-3}$ mg cm^{-2} h^{-1}, with inhibition efficiency increasing from 60% to 94% under the same conditions. The steady increase in inhibition efficiency with inhibitor concentration suggests enhanced adsorption of CaO/SiO_2 nanoparticles onto the steel surface, leading to more effective blocking of active corrosion sites.

Table 1: Corrosion Parameters of Low-Carbon Steel in 15% HCl and 15% H_2SO_4 Solutions in the Absence and Presence of Different Concentrations of Synthesized CaO/SiO_2 Nanocomposite Inhibitor at Different Temperatures

Media	CaO/SiO_2 Nanocomposite (mg/L)	303 K			313 K			323 K			333 K		
		CR (mg $cm^{-2}h^{-1}$) $\times10^{-3}$	θ	IE (%)	CR (mg $cm^{-2}h^{-1}$) $\times10^{-3}$	θ	IE (%)	CR (mg $cm^{-2}h^{-1}$) $\times10^{-3}$	θ	IE (%)	CR (mg $cm^{-2}h^{-1}$) $\times10^{-3}$	θ	IE (%)
15% H_2SO_4	2	2.85	0.42	42	4.25	0.32	32	5.95	0.24	24	7.80	0.18	18
	4	2.35	0.52	52	3.60	0.43	43	4.90	0.36	36	6.75	0.28	28
	6	1.70	0.65	65	2.85	0.55	55	3.85	0.48	48	5.40	0.39	39
	8	1.10	0.77	77	2.05	0.67	67	2.85	0.61	61	4.20	0.52	52
	10	0.65	0.86	86	1.35	0.78	78	2.00	0.69	69	3.10	0.63	63
	Blank	4.90	–	–	7.10	–	–	9.25	–	–	12.30	–	–
15% HCl	2	2.20	0.60	60	3.40	0.51	51	4.80	0.39	39	6.90	0.29	29
	4	1.70	0.69	69	2.75	0.61	61	3.90	0.52	52	5.75	0.42	42
	6	1.10	0.80	80	1.95	0.75	75	3.00	0.65	65	4.60	0.53	53
	8	0.65	0.90	90	1.25	0.84	84	2.10	0.77	77	3.60	0.63	63
	10	0.35	0.94	94	0.80	0.90	90	1.45	0.85	85	2.70	0.73	73
	Blank	5.50	–	–	8.00	–	–	10.20	–	–	13.50	–	–

The greater inhibition efficiency observed in HCl compared with H_2SO_4 is ascribed to the distinct adsorption characteristics of chloride and sulfate ions. Chloride ions are smaller and more weakly hydrated, allowing them to approach the steel surface more closely and promote the adsorption of inhibitor species (Zamindar *et al.,* 2024; Chen *et al.,* 2022). Conversely, sulfate ions exhibit a larger hydration shell and compete more effectively for adsorption sites, which may weaken the interaction between the nanocomposite and the metal surface (Yang *et al.,* 2018). Consequently, the CaO/SiO_2 nanocomposite developed a more compact and protective layer in the HCl medium.

The effect of temperature revealed that the inhibition efficiency declined as the temperature rose from 303 to 333 K. At a CaO/SiO_2 concentration of 10 mg/L, the inhibition efficiency declined from 86% to 63% in H_2SO_4 and from 94% to 73% in HCl. The decline in efficiency at higher temperatures implies partial desorption of the adsorbed nanocomposite film from the steel surface, thereby exposing a larger portion of the metal to the acidic environment (Hasanin & Al Kiey, 2023). This behaviour suggests that the adsorption of CaO/SiO_2 nanoparticles is governed predominantly by physical adsorption, whereas chemical interactions between oxygen-containing surface groups and iron atoms may also enhance the stability of the protective film.

The present results are consistent with previous studies on oxide-based nanomaterials as corrosion inhibitors. Thakur *et al.* (2023) reported that nanomaterials exhibit improved corrosion protection due to their large surface area, which promotes adsorption and formation of a compact barrier film on metal surfaces. Their findings support the enhanced inhibition performance observed for CaO/SiO_2 nanocomposite in the present work. Similarly, AbdElRhiem *et al.* (2025) demonstrated that inorganic nanoparticles containing oxygen-bearing functional groups can significantly reduce corrosion by blocking active anodic and cathodic sites.

The superior performance of the CaO/SiO_2 nanocomposite can be explained by the formation of a protective adsorbed film through interaction between the nanoparticle surface and the steel substrate. The adsorbed film prevents direct contact between the corrosive medium and the metal surface, thereby reducing anodic dissolution:

$$Fe \rightarrow Fe^{2+} + 2e^-$$

and suppressing cathodic hydrogen evolution:

$$2H^+ + 2e^- \rightarrow H_2$$

Consequently, the corrosion process is significantly inhibited.

3.2 Langmuir Adsorption Isotherm Behaviour for CaO/SiO_2 Nanocomposite on Low Carbon Steel in 15% H_2SO_4 and 15% HCl Media

The adsorption characteristics of the CaO/SiO_2 nanocomposite on the low-carbon steel surface in 15% H_2SO_4 and 15% HCl media were investigated using the Langmuir adsorption isotherm by plotting Cinh/θ against Cinh at 303, 313, 323, and 333 K. The resulting plots (Figures 1 and 2) exhibited excellent linearity across the investigated inhibitor concentration range (2–10 mg/L), demonstrating that the adsorption of the CaO/SiO_2 nanocomposite conforms to the Langmuir adsorption model. The close agreement with the Langmuir isotherm implies that adsorption proceeds through the formation of a monolayer protective film on the steel surface, in which inhibitor molecules adsorb onto the available active corrosion sites with minimal interactions between neighbouring adsorbed species. The Langmuir adsorption model is expressed as (Azizian *et al.,* 2018):

$$\frac{C_{inh}}{\theta} = \frac{1}{K_{ads}} + C_{inh}$$

where Cinh represents inhibitor concentration, θ represents the fraction of the steel surface covered by inhibitor molecules, and Kads is the adsorption equilibrium constant. The linear relationship between Cinh/θ and Cinh demonstrates that the surface coverage increases steadily with increasing CaO/SiO_2 nanocomposite concentration owing to the increased availability of adsorbing species in the corrosive environment.

In 15% H_2SO_4 medium, the Langmuir plots (Figure 1) demonstrated excellent linearity at all studied temperatures. At lower temperature (303 K), the plot displayed lower Cinh/θ values, implying stronger adsorption of the CaO/SiO_2 nanocomposite on the steel surface. Increasing the temperature to 333 K led to elevated Cinh/θ values, indicating a decrease in adsorption strength. This behaviour is consistent with the observed decline in inhibition efficiency from 86% at 303 K to 63% at 333 K for a 10 mg/L inhibitor concentration. The loss of surface protection at elevated temperature can be ascribed to enhanced molecular motion, which diminishes adsorption forces and facilitates partial desorption of the adsorbed inhibitor film. This observation is consistent with the results reported by Selvi *et al.* (2020). The adsorption mechanism in sulfuric acid solution is ascribed to the interaction between active sites on the steel surface and oxygen-containing groups in the nanocomposite, such as Si–OH, Si–O–Si, and Ca–O functional groups. These surface groups act as electron-rich centres that engage with iron atoms, leading to the development of an adsorbed protective layer (Zamindar *et al*., 2024). This layer limits the penetration of sulfate ions to the steel surface and suppresses both anodic iron corrosion and cathodic hydrogen evolution reactions.

For 15% HCl medium, a similar linear correlation (Figure 2) was observed, supporting Langmuir adsorption behaviour. However, the HCl system displayed relatively lower Cinh/θ values

than H_2SO_4 at equivalent inhibitor concentrations and temperatures, implying stronger adsorption of the CaO/SiO_2 nanocomposite on the steel surface. This stronger adsorption behaviour is consistent with the higher inhibition efficiency recorded in HCl medium, where a maximum efficiency of 94% at 303 K was achieved compared with 86% in H_2SO_4.

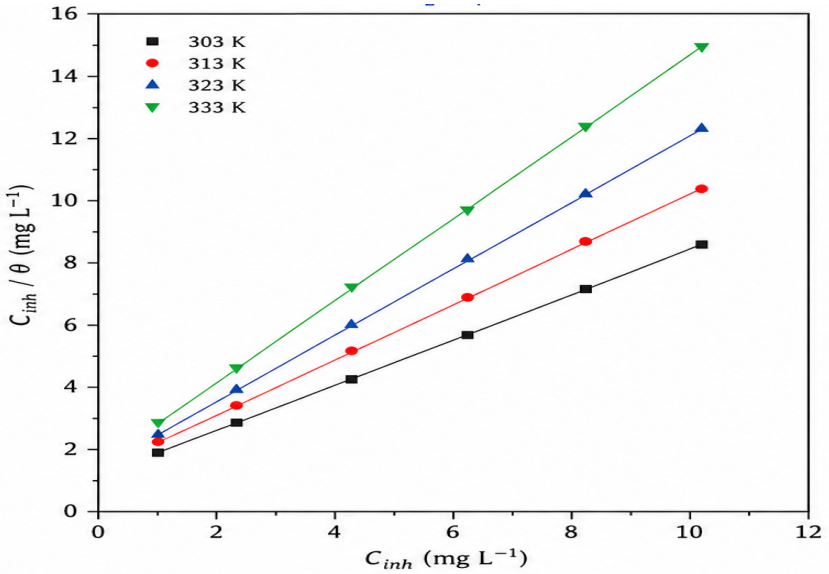

Figure 1: Langmuir adsorption isotherm plots of the CaO/SiO_2 nanocomposite on low-carbon steel in 15% H_2SO_4 solutions at different temperatures.

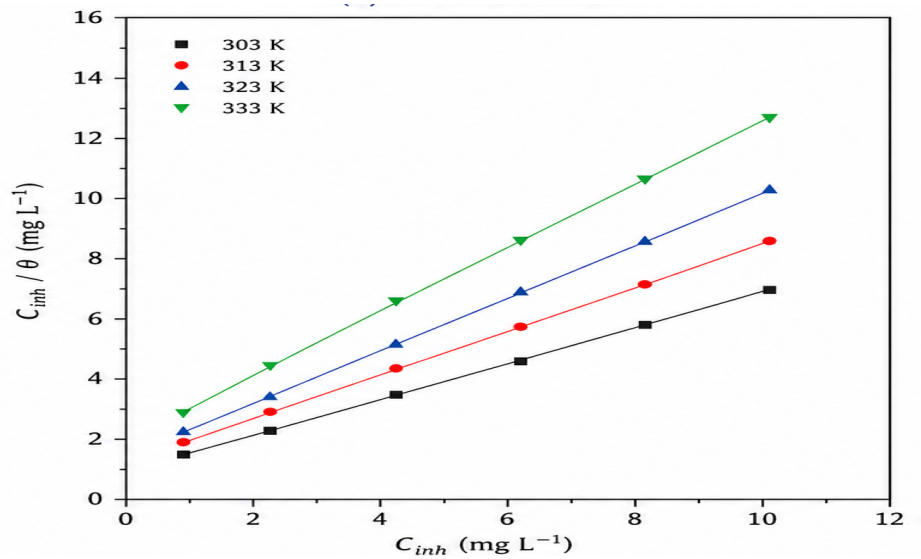

Figure 2: Langmuir adsorption isotherm plots of the CaO/SiO_2 nanocomposite on low-carbon steel in 15% HCl solutions at different temperatures.

The improved adsorption in hydrochloric acid may be ascribed to the effect of chloride ions. Chloride ions exhibit a smaller ionic size and lower hydration energy than sulfate ions, facilitating closer access to the steel surface. The presence of chloride ions may facilitate the adsorption of CaO/SiO_2 nanoparticles by altering the surface charge and strengthening the affinity between the inhibitor species and the metal substrate. Conversely, sulfate ions are highly hydrated and compete strongly for adsorption sites, thereby limiting the ability of the inhibitor molecules to form a compact protective film. The proposed adsorption mechanism of the CaO/SiO_2 nanocomposite can be summarized as follows:

(i) Adsorption of CaO/SiO_2 nanoparticles onto active corrosion sites:

$$Steel + CaO/SiO_2 \rightarrow Steel - CaO/SiO_2(ads)$$

(ii) Formation of a protective barrier film that prevents penetration of acidic ions.

(iii) Suppression of anodic and cathodic corrosion reactions.

The combined adsorption and barrier effects reduce the corrosion rate and improve protection efficiency.

3.3 *Thermodynamic Adsorption Behaviour and Corrosion Inhibition Mechanism of CaO/SiO_2 Nanocomposite on Low Carbon Steel in 15% H_2SO_4 and 15% HCl Media*

The thermodynamic adsorption parameters (Table 2) derived from the Langmuir adsorption isotherm offer valuable insight into the adsorption of the CaO/SiO_2 nanocomposite on the low-carbon steel surface in 15% H_2SO_4 and 15% HCl acidic environments. The adsorption parameters, namely the adsorption equilibrium constant (Kads), Gibbs free energy change ($\Delta G°$), enthalpy change ($\Delta H°$), entropy change ($\Delta S°$), and correlation coefficient (R^2), were employed to characterize the nature, spontaneity, and stability of the adsorption process. The correlation coefficient values recorded for both acidic media (R^2 = 0.978–0.995) demonstrate a strong correlation between the experimental data and the Langmuir adsorption model. This finding confirms that the adsorption of the CaO/SiO_2 nanocomposite onto the low-carbon steel surface proceeds via a monolayer adsorption mechanism, in which the inhibitor nanoparticles adsorb onto active corrosion sites with minimal interaction among neighbouring adsorbed species. The close fit to the Langmuir model implies that the inhibition efficiency of the CaO/SiO_2 nanocomposite is predominantly governed by the adsorption of the inhibitor species on the metal surface.

The adsorption equilibrium constant (K_{ads}) values revealed strong interaction between the nanocomposite and the steel surface. In 15% H_2SO_4 medium, Kads decreased from 1.860 L mg^{-1} at 303 K to 0.720 L mg^{-1} at 333 K, while in 15% HCl medium, it decreased from 2.950 L mg^{-1} to 1.020 L mg^{-1} within the same temperature range. The higher Kads values in HCl indicate stronger adsorption of the CaO/SiO_2 nanocomposite onto the steel surface, consistent with the higher inhibition efficiency recorded in HCl medium (94%) compared with H_2SO_4 (86%) at 303 K. The decrease in Kads with increasing temperature indicates that adsorption becomes less favourable at elevated temperatures due to increased molecular motion and partial desorption of the adsorbed inhibitor layer. This observation is similar to that of Ituen *et al.* (2016), who reported that adsorption equilibrium constants decrease with increasing temperature, reflecting a predominantly physical adsorption process and reduced inhibitor stability on the metal surface at higher temperatures. The variation in adsorption strength between the two-acid media can be related to the nature of the aggressive ions present. In hydrochloric acid solution, chloride ions are smaller, less strongly hydrated, and possess greater adsorption ability, enabling easier interaction between the inhibitor species and the steel surface (Chen *et al.,* 2022). This promotes the formation of a compact protective film. However, sulfate ions in sulfuric acid possess a larger hydrated structure and compete strongly for adsorption sites, thereby reducing the extent of CaO/SiO_2 adsorption (Kolics & Wieckowski, 2001). Consequently, weaker adsorption and lower inhibition efficiency were observed in H_2SO_4 medium.

The Gibbs free energy values ($\Delta G°$) derived for all conditions were negative, confirming that the adsorption process is spontaneous. In 15% H_2SO_4, $\Delta G°$ values ranged from −8.05 kJ mol^{-1} at 303 K to −7.26 kJ mol^{-1} at 333 K, whereas in 15% HCl, the values ranged from −9.36 kJ mol^{-1} to −8.31 kJ mol^{-1}. The more negative $\Delta G°$ values in HCl confirm a stronger and more favourable adsorption

process. In general, ΔG° values less negative than approximately −20 kJ mol^{-1} suggest physical adsorption, while strongly negative values approaching −40 kJ mol^{-1} indicate chemical adsorption. Therefore, the derived ΔG° values imply that adsorption of the CaO/SiO$_2$ nanocomposite occurs mainly through physisorption, driven by electrostatic attraction between charged inhibitor species and the metal surface. However, the contribution of weak chemical interactions cannot be ruled out due to the presence of oxygen-containing functional groups such as Si–OH, Si–O–Si, and Ca–O, which may engage with iron atoms to reinforce the protective layer. Similarly, Adamu *et al.* (2025) reported that effective corrosion inhibitors exhibit spontaneous adsorption characterized by negative Gibbs free energy values. They further explained that intermediate negative ΔG° values indicate physical adsorption, which is consistent with the adsorption mechanism identified for the CaO/SiO$_2$ nanocomposite.

The enthalpy change values were negative in both media, with ΔH° = −31.42 kJ mol^{-1} for 15% H$_2$SO$_4$ and −27.85 kJ mol^{-1} for 15% HCl. The negative values confirm that the adsorption process is exothermic, indicating that heat is released when CaO/SiO$_2$ nanoparticles adsorb onto the steel surface. Therefore, increasing temperature reduces adsorption stability, accounting for the decline in inhibition efficiency at elevated temperatures. The magnitude of the enthalpy values also supports a mainly physical adsorption process with possible involvement of chemical interactions between the nanocomposite and the steel substrate. This observation is similar to that of Sahmoune (2019), who reported that negative enthalpy values indicate an exothermic adsorption process.

The entropy change values were negative for both acidic systems, with values of −77.21 J mol^{-1} K^{-1} in H$_2$SO$_4$ and −61.54 J mol^{-1} K^{-1} in HCl. The negative ΔS° values reflect a reduction in randomness at the metal–solution interface during adsorption (Liu & Lee, 2014). This occurs because freely dispersed CaO/SiO$_2$ nanoparticles become organized on the steel surface to form an ordered protective barrier layer. The more negative entropy value in H$_2$SO$_4$ implies a higher degree of ordering during adsorption, which may arise from stronger competition between sulfate ions and inhibitor species for adsorption sites.

Table 2: Thermodynamic Parameters from the Langmuir Adsorption Isotherm for Low-Carbon Steel in 15% HCl and 15% H$_2$SO$_4$ Solutions Containing Synthesized CaO/SiO$_2$ Nanocomposite Inhibitor at Different Temperatures

Acid Medium	Temperature (K)	Kads (L mg^{-1})	ln Kads	ΔG° (kJ mol^{-1})	ΔH° (kJ mol^{-1})	ΔS° (J mol^{-1} K^{-1})	R^2
15% H$_2$SO$_4$	303	1.860	0.621	−8.05	−31.42	−77.21	0.991
	313	1.410	0.344	−7.81	−31.42	−77.21	0.987
	323	1.020	0.020	−7.52	−31.42	−77.21	0.983
	333	0.720	−0.329	−7.26	−31.42	−77.21	0.978
15% HCl	303	2.950	1.082	−9.36	−27.85	−61.54	0.995
	313	2.180	0.779	−9.01	−27.85	−61.54	0.992
	323	1.540	0.432	−8.68	−27.85	−61.54	0.989
	333	1.020	0.020	−8.31	−27.85	−61.54	0.985

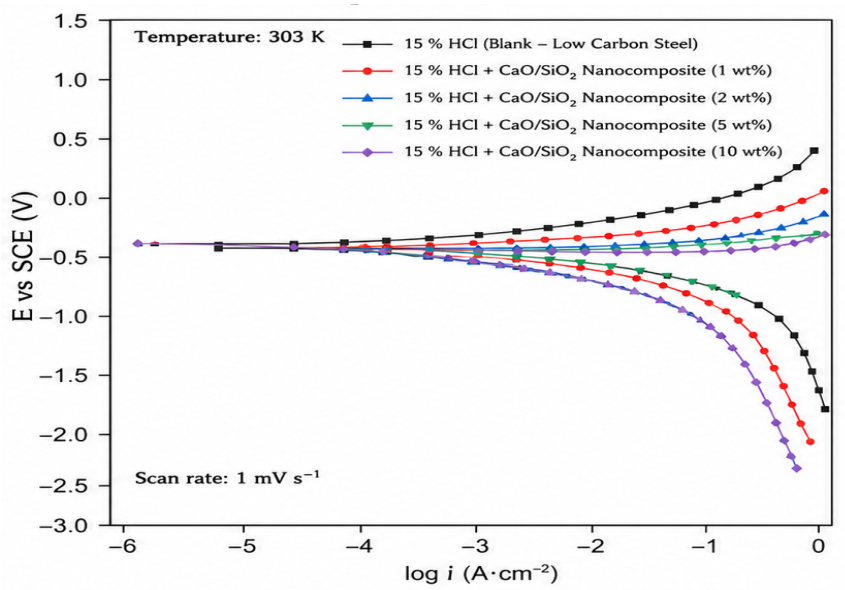

Figure 3: Polarization curve of variable concentrations of CaO/SiO_2 Nanocomposite in15 % HCl solution at 303 K

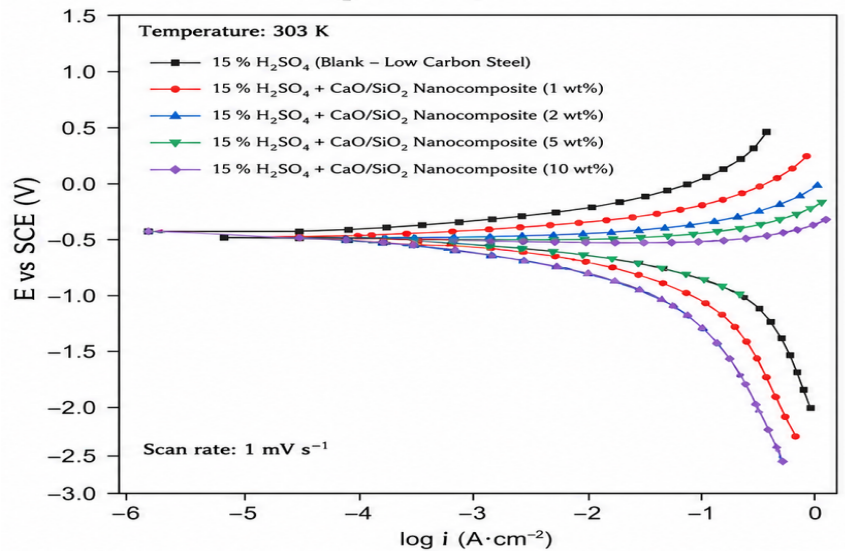

Figure 4: Polarization curve of variable concentrations of CaO/SiO_2 Nanocomposite in15 % H_2SO_4 solution at 303 K

3.4 *Potentiodynamic Polarization Behaviour*

The potentiodynamic polarization curves (Figure 3 and 4) obtained for low carbon steel in 15% HCl and 15% H_2SO_4 solutions containing CaO/SiO_2 nanocomposite demonstrate that the nanocomposite effectively reduces the electrochemical corrosion reactions of steel. The inhibited systems exhibited lower anodic and cathodic current densities compared with the uninhibited samples, confirming the protective action of CaO/SiO_2 nanocomposite through adsorption and formation of a barrier layer on the metal surface. The observed decrease in corrosion current density with increasing CaO/SiO_2 concentration agrees with the findings of Okon *et al.* (2025), who reported that nanoparticle-based inhibitors reduce corrosion activity by adsorbing onto the metal surface and blocking active corrosion sites. Similar inhibition behaviour was observed by Avdeev *et al.* (2024), where protective films formed by inhibitor molecules significantly reduced both anodic metal dissolution and cathodic hydrogen evolution reactions.

The suppression of both anodic and cathodic branches in the present study indicates that CaO/SiO_2 nanocomposite acts as a mixed-type corrosion inhibitor. This behaviour is consistent with the work of Numin *et al*. (2026), who reported that effective inhibitors reduce corrosion by simultaneously controlling anodic dissolution of iron and cathodic reduction processes. The absence of a major shift in corrosion potential after inhibitor addition further confirms that the nanocomposite does not preferentially inhibit only one electrochemical reaction. The improved inhibition efficiency of CaO/SiO_2 nanocomposite compared with the blank solution can be associated with the high surface area and adsorption ability of the nanoparticles. Borisova *et al*. (2011) reported that silica nanoparticles enhance corrosion protection due to their high surface energy, large specific surface area, and ability to form compact protective layers. In the present study, the incorporation of CaO with SiO_2 likely enhanced this effect by providing additional active adsorption centres, improving surface coverage and stability of the protective film.

Table 3: Potentiodynamic polarization parameters obtained from Tafel plots for low carbon steel in 15% HCl and 15% H_2SO_4 solutions containing synthesized CaO/SiO_2 nanocomposite at 303 K

System	Corrosion rate (mpy)	$-E_{corr}$ (mV vs SCE)	I_{corr} (μA cm^{-2})	β_a (mV dec^{-1})	β_c (mV dec^{-1})	Inhibition efficiency (IE %)
15% HCl (Blank – Low carbon steel)	1.416×10^3	388.0	3100	562.3×10^{-3}	1.00×10^{15}	–
15% HCl + CaO/SiO_2 nanocomposite (2%)	394.1	506.0	862.0	408.4×10^{-3}	270.6×10^{-3}	72.20
15% HCl + CaO/SiO_2 nanocomposite (10%)	842.8	448.0	1840	522.4×10^{-3}	1.00×10^{15}	40.65
15% H_2SO_4 (Blank – Low carbon steel)	66.17	1.05	145.0	305.6×10^{-3}	547.8×10^{-3}	–
15% H_2SO_4 + CaO/SiO_2 nanocomposite (2%)	59.09	1.06	129.0	312.1×10^{-3}	572.1×10^{-3}	11.03
15% H_2SO_4 + CaO/SiO_2 nanocomposite (10%)	44.23	1.06	96.8	266.5×10^{-3}	471.5×10^{-3}	33.24

The electrochemical parameters (Table 3) derived in this study for low-carbon steel in the presence of the CaO/SiO_2 nanocomposite are in agreement with previous reports on nanoparticle-based corrosion inhibitors. The decrease in corrosion current density (Icorr) and corrosion rate following the incorporation of the CaO/SiO_2 nanocomposite confirms that the nanocomposite effectively inhibits the electrochemical dissolution of steel in acidic environments.

The elevated corrosion current density (3100 μA cm^{-2}) recorded for low-carbon steel in 15% HCl without inhibitor reflects severe corrosion due to the aggressive attack of chloride ions, which enhance anodic iron dissolution and cathodic hydrogen evolution. Similar behaviour was reported by Saha *et al*. (2015), who observed that mild steel corrosion in acidic solutions is significantly suppressed when inhibitor species adsorb on the steel surface and block active corrosion sites. The reduction of Icorr to 862 μA cm^{-2} and the associated inhibition efficiency of 72.20% at 2% CaO/SiO_2 nanocomposite concentration demonstrate efficient surface protection.

The higher inhibition efficiency recorded in this study is consistent with the findings of Alao (2022), who reported that nanostructured inhibitors improve corrosion resistance via adsorption and

the formation of protective films. The CaO/SiO_2 nanocomposite likely adsorbs onto the steel surface via interactions between oxide functional groups and iron atoms, creating a barrier that restricts the penetration of H^+ and Cl^- ions. The decline in corrosion rate from 1.416×10^3 mpy (blank) to 394.1 mpy (2% CaO/SiO_2) in HCl is comparable with the trend reported for other oxide nanoparticles. Chen *et al*. (2025) reported that the inclusion of silica nanoparticles enhances corrosion resistance due to their high surface area, strong adsorption ability, and capacity to fill micro-defects on metal surfaces. The superior performance of CaO/SiO_2 compared with individual oxides may be ascribed to the synergistic effect of CaO and SiO_2, where silica offers adsorption sites while CaO improves surface affinity and film stability.

However, the decline in inhibition efficiency from 72.20% (2%) to 40.65% (10%) in HCl implies that excessive nanoparticle concentration may induce aggregation, reducing active adsorption sites. Similar concentration-dependent behaviour was reported by Zarrouk *et al*. (2012), where increased inhibitor concentrations did not always yield proportional improvement due to aggregation of inhibitor species and diminished affinity with the metal surface.

In 15% H_2SO_4 solution, the corrosion current density declined from 145 µA cm^{-2} (blank) to 129 µA cm^{-2} and 96.8 µA cm^{-2} for 2% and 10% CaO/SiO_2 nanocomposite, respectively. The maximum inhibition efficiency of 33.24% at 10% concentration suggests that sulfate ions demand higher inhibitor concentration for effective surface coverage. This observation agrees with Chen *et al*. (2022), who reported that corrosion inhibition efficiency is governed by the affinity between inhibitor molecules and the characteristics of the acidic electrolyte.

The changes in Tafel slopes (βa and βc) after inhibitor incorporation confirm that the CaO/SiO_2 nanocomposite affects both anodic and cathodic reactions. Similar mixed-type inhibition behaviour was reported by Fekry & Ameer (2010), where corrosion inhibitors diminished both metal dissolution and hydrogen evolution without appreciably shifting the corrosion potential. The Nyquist impedance behaviour further corroborates the polarization results. The larger semicircle diameter recorded for inhibited steel compared with the blank sample signifies increased charge transfer resistance (Rct) and reduced corrosion activity. Similar impedance behaviour was reported by Pradityana *et al*. (2026), who ascribed the increased semicircle diameter to the development of an adsorbed layer that restricts charge transfer between the metal and electrolyte. The improved impedance behaviour at 10% CaO/SiO_2 concentration in H_2SO_4 indicates enhanced adsorption and a more compact protective film formation. This is consistent with the findings of Oreko & Okuma (2025), who reported that oxide-based nanomaterials improve corrosion resistance by increasing surface coverage and reducing electrochemical reaction sites.

The Nyquist plots (Figure 5 and 6) of low-carbon steel in 15% HCl and 15% H_2SO_4 containing CaO/SiO_2 nanocomposite show that both acid type and inhibitor concentration strongly influence electrochemical behaviour. The blank H_2SO_4 solution exhibits a smaller capacitive loop than HCl, indicating lower charge-transfer resistance (Rct) and higher corrosion rate, consistent with the stronger corrosivity of sulfate media reported in literature (Solmaz *et al*., 2008; Lame *et al*., 2024; Liu *et al*., 2024).

In HCl, Rct increases up to 2 wt% CaO/SiO_2, suggesting effective adsorption and formation of a protective film, but decreases at 10 wt%, indicating an optimum concentration beyond which nanoparticle aggregation and non-uniform surface coverage reduce protection. In contrast, in H_2SO_4, Rct increases steadily with concentration, reflecting progressive adsorption and more stable film formation under sulfate conditions. A similar observation was reported by AbdElRhiem *et al*. (2025).

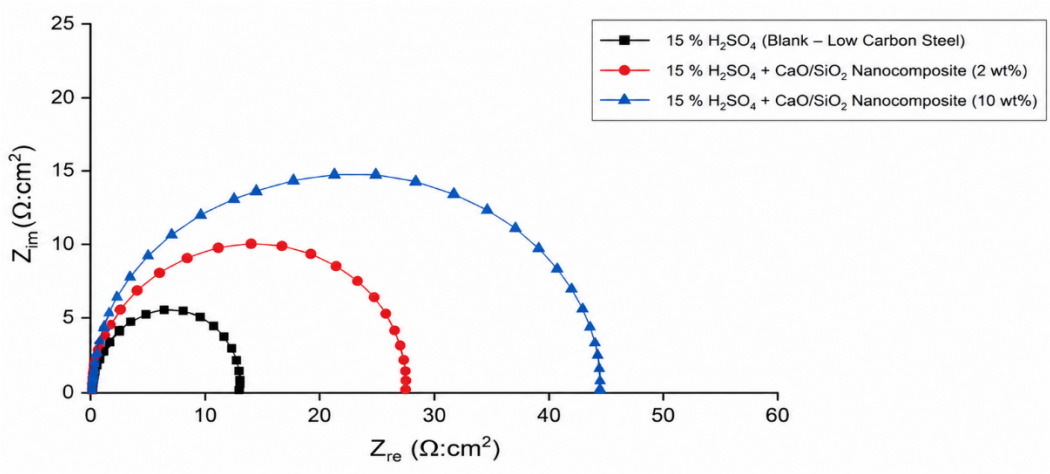

Figure 5: Nyquist plot of variable concentrations of CaO/SiO_2 nanocomposite in 15 % HCl solution at 303 K.

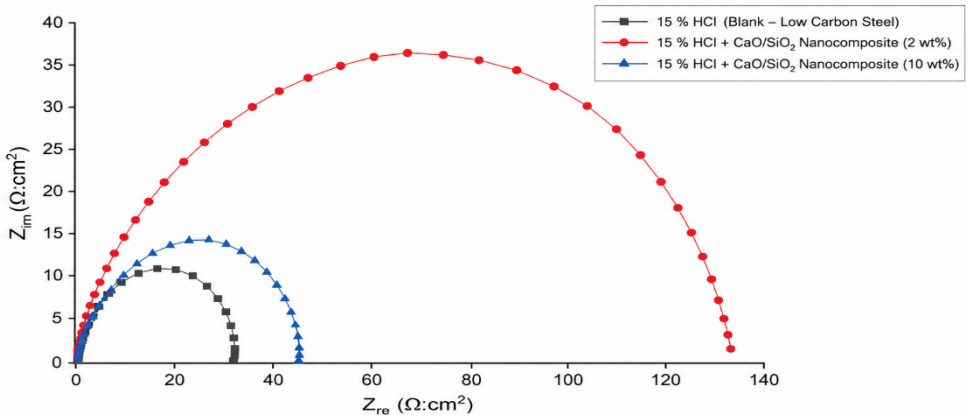

Figure 6: Nyquist plot of variable concentrations of CaO/SiO_2 nanocomposite in 15 % H_2SO_4 solution at 303 K.

The variations in corrosion inhibition are attributed to differences in anion behaviour. Chloride ions promote initial adsorption at low inhibitor concentrations, whereas sulfate ions necessitate greater inhibitor concentrations for adequate surface coverage. These findings are consistent with those reported by Akrout *et al.* (2025). At elevated inhibitor concentrations, nanoparticle aggregation and film heterogeneity facilitate the formation of diffusion pathways for corrosive ions, resulting in reduced inhibition efficiency in HCl. The Electrochemical Impedance Spectroscopy (EIS) results (Table 4) demonstrate that the CaO/SiO_2 nanocomposite suppressed the corrosion of low-carbon steel in both 15% HCl and 15% H_2SO_4 by enhancing the charge-transfer resistance (Rct) and reducing the constant phase element (Q), reflecting the adsorption of the inhibitor and the development of a surface barrier film. In 15% HCl, the Rct rose from 36.49 Ω cm² for the blank solution to 116.40 Ω cm² at 2 wt% CaO/SiO_2, yielding an inhibition efficiency of 68.65%. The lower Q value reflects diminished electrochemical activity resulting from surface coverage by the nanocomposite. At 10 wt%, the Rct declined, suggesting that higher nanoparticle loading promoted agglomeration and non-uniform film formation, consequently leading to a decline in inhibition efficiency. These findings are consistent with those reported by Habibi *et al.* (2026).

In 15% H_2SO_4, the Rct rose from 169.00 Ω cm² for the blank solution to 224.80 Ω cm² and 236.80 Ω cm² at 2 wt% and 10 wt%, respectively, reflecting a gradual improvement in corrosion resistance as the inhibitor concentration increased. This behaviour suggests more effective adsorption

and improved integrity of the surface film in sulfuric acid. This trend is consistent with the results reported by Hermas *et al.* (2029). Larger Nyquist semicircles observed for the inhibited systems, accompanied by lower Q values and α values of 0.68–0.75, signify diminished charge transfer and non-ideal capacitive behaviour arising from adsorption on a heterogeneous steel surface. Collectively, these findings show that the CaO/SiO_2 nanocomposite functions as an effective corrosion inhibitor through adsorption and barrier-film formation, exhibiting optimum performance at 2 wt% in HCl and sustained improvement up to 10 wt% in H_2SO_4.

Table 4: Electrochemical Impedance Spectroscopy (EIS) parameters of low carbon steel in 15% HCl and 15% H_2SO_4 solutions containing synthesized CaO/SiO_2 nanocomposite at 303 K

System	Rs (Ω cm²)	Rct cm²)	(Ω Q × 10⁻³ (S sⁿ cm⁻²)	α	Goodness of fit (χ²)	IE (%)
15% HCl (Blank – Low carbon steel)	2.880	36.49	1.290	0.74	1.79×10^{-3}	–
15% HCl + CaO/SiO_2 nanocomposite (2 wt%)	1.229	116.40	0.855	0.74	1.50×10^{-3}	68.65
15% HCl + CaO/SiO_2 nanocomposite (10 wt%)	1.004	38.75	1.080	0.75	2.96×10^{-3}	5.83
15% H_2SO_4 (Blank – Low carbon steel)	7.545	169.00	3.150	0.72	1.74×10^{-3}	–
15% H_2SO_4 + CaO/SiO_2 nanocomposite (2 wt%)	11.510	224.80	1.840	0.74	1.54×10^{-3}	24.82
15% H_2SO_4 + CaO/SiO_2 nanocomposite (10 wt%)	3.669	236.80	3.300	0.68	8.02×10^{-3}	28.63

3.5 SEM and EDX Analysis

SEM images (Figure 7a, b and 8a, b) reveal extensive surface degradation of uninhibited low-carbon steel in acidic media, characterized by irregular, heterogeneous morphology, deep pits, and corrosion products, reflecting intense anodic dissolution and hydrogen evolution. In contrast, inhibited samples exhibit comparatively more uniform surfaces with fewer pits and a more homogeneous morphology, demonstrating the corrosion-inhibiting effect of the CaO/SiO_2 nanocomposite. In the inhibited specimens, granular and spherical formations are evident, arising from nanocomposite particles forming a compact surface layer that restricts electrolyte penetration. Slightly denser particulate coverage is evident in H_2SO_4 (Figure 8a, b) compared to HCl (Figure 7a, b), likely due to differences in anion behaviour and adsorption characteristics, though both media exhibit pronounced surface protection.

EDX analysis (9a, b) reveals the characteristic signals of Ca, Si, and O on the inhibited steel surfaces, supporting the adsorption of the CaO/SiO_2 nanocomposite onto the metal substrate. The appearance of these elemental peaks, which are absent or significantly weaker in the uninhibited sample, further substantiates the formation of a surface-adhered inhibitor layer. In addition, a marked reduction in the Fe peak intensity is observed, reflecting effective surface coverage and partial shielding of the steel substrate by the protective film.

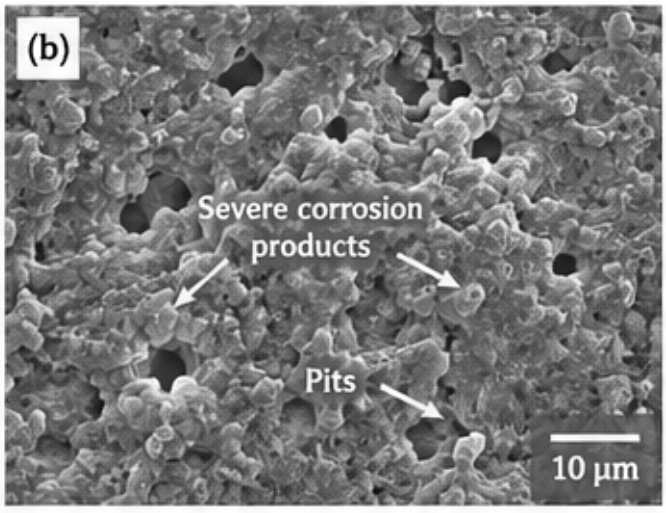

Figure 7a: SEM Micrograph of Low-Carbon Steel after Immersion in 15% HCl Showing Severe Corrosion Products and Pitting

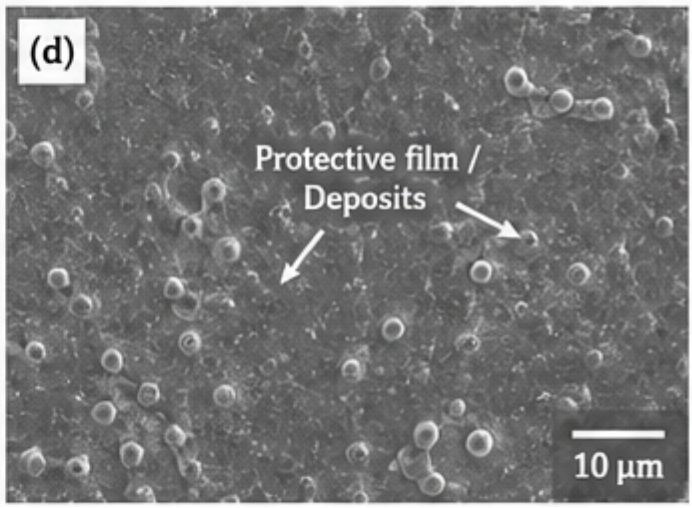

Figure 7b: Surface Morphology of Low-Carbon Steel Showing Formation of Protective Film/Deposits After addition of CaO/SiO_2 Nanocomposite in 15% HCl

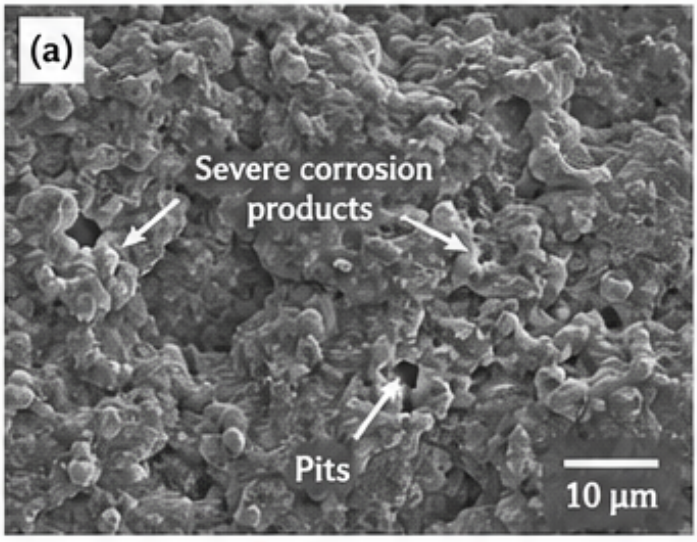

Figure 8a: SEM Micrograph of Low-Carbon Steel after Immersion in 15% H_2SO_4 Showing Severe Corrosion Products and Pitting

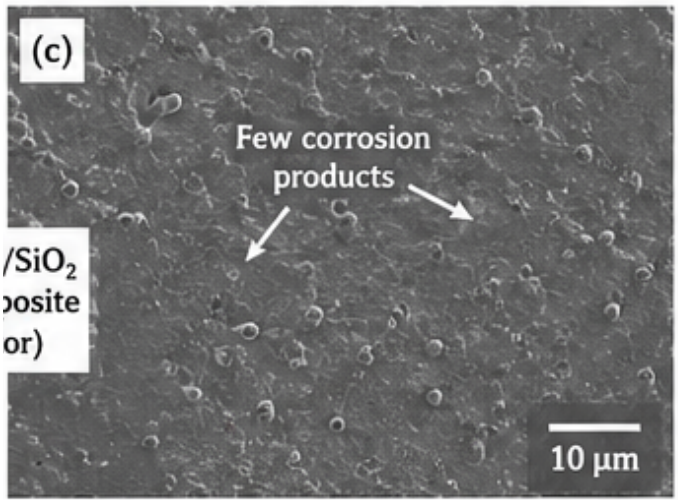

Figure 8b: Surface Morphology of Low-Carbon Steel Showing Formation of Protective Film/Deposits After addition of CaO/SiO_2 Nanocomposite in 15% H_2SO_4

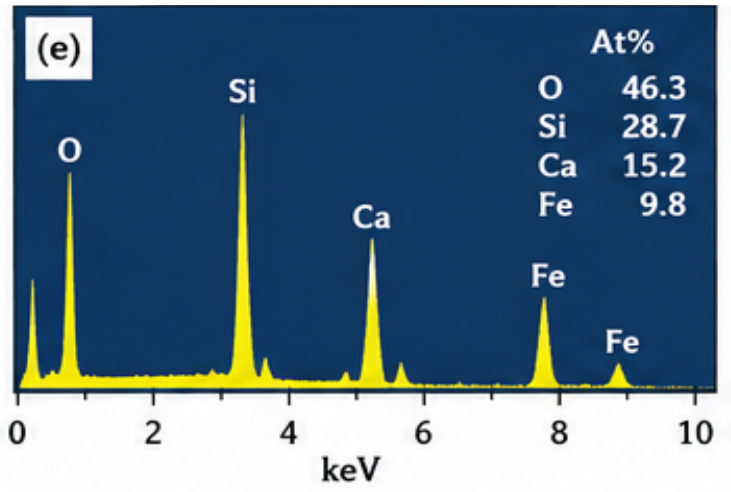

Figure 9a: Energy-Dispersive X-ray (EDX) Spectrum of Low-Carbon Steel Surface after Treatment with CaO/SiO_2 Nanocomposite in 15% H_2SO_4 Solution Showing the Presence of Ca, Si, O, and Fe Elements.

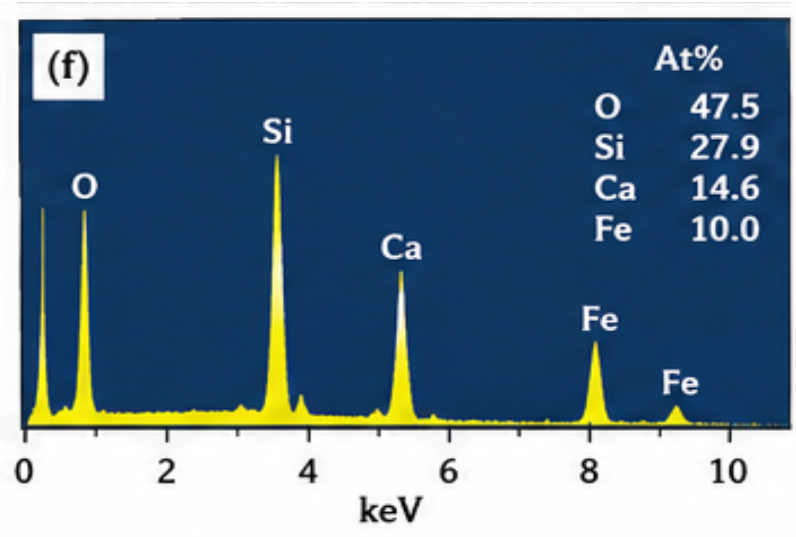

Figure 9b: Energy-Dispersive X-ray (EDX) Spectrum of Low-Carbon Steel Surface after Treatment with CaO/SiO_2 Nanocomposite in 15% HCl Solution Showing the Presence of Ca, Si, O, and Fe Elements.

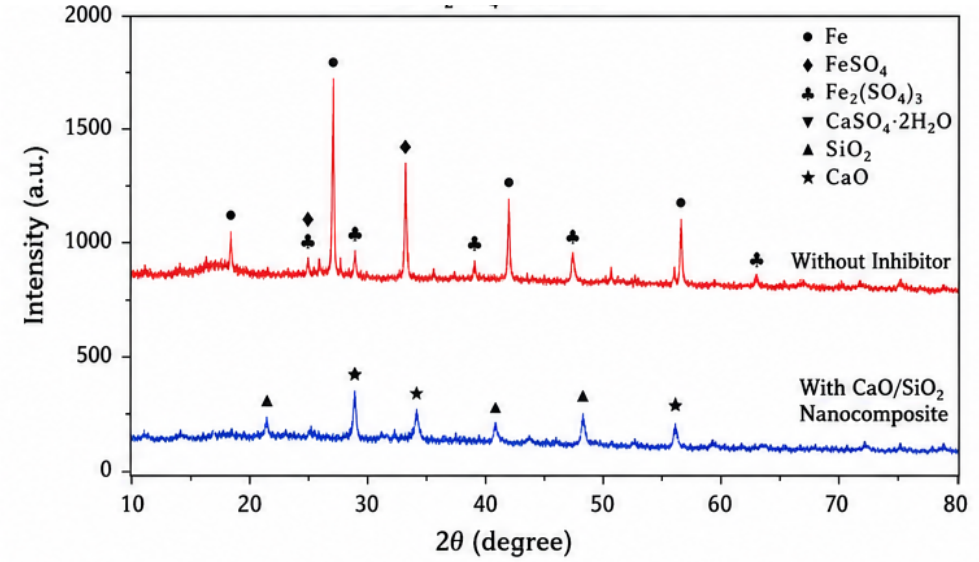

Figure 10a. XRD analysis (corrosion product on low carbon steel) in 15 % H_2SO_4 solution

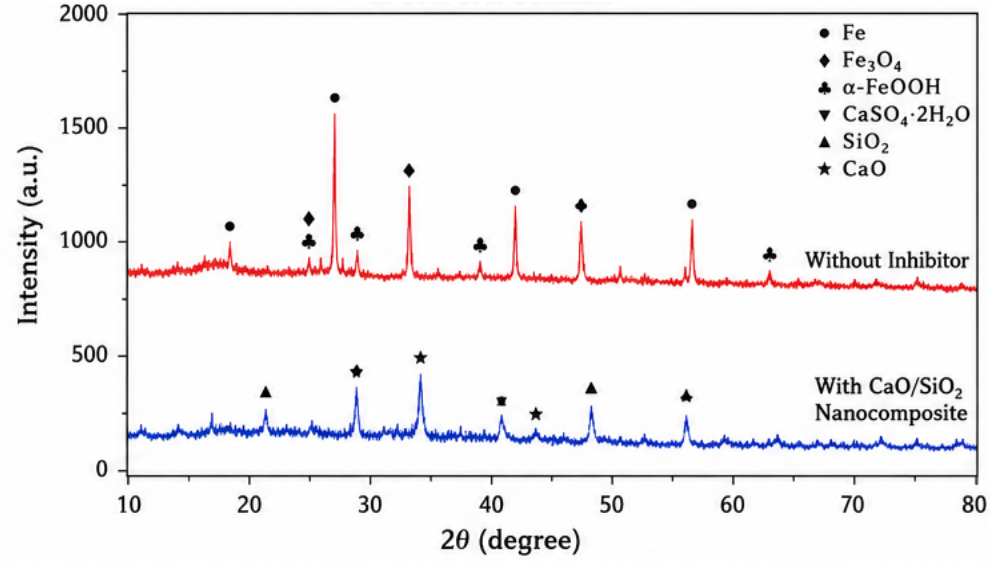

Figure 10b: XRD analysis (corrosion product on low carbon steel) in 15 % HCl solution

3.6 Structural Evaluation by X-ray Diffraction (XRD)

The XRD profile of uninhibited low-carbon steel (Figure 10a, b) exhibits sharp, high-intensity reflections (≈1500–1800 a.u.), reflecting highly ordered corrosion products. Alongside α-Fe, diffraction peaks corresponding to $FeSO_4$, $Fe_2(SO_4)_3$, Fe_3O_4, and α-FeOOH are detected, evidencing severe corrosion and the development of crystalline oxide and sulfate phases in acidic media, in agreement with SEM observations. Following incorporation of the CaO/SiO_2 nanocomposite, diffraction intensity decreases markedly (<500 a.u.), while reflections associated with corrosion products are substantially suppressed, indicating a pronounced reduction in corrosion activity. Weak, broadened peaks corresponding to CaO and SiO_2 emerge, implying the development of an amorphous or nanocrystalline protective surface film on the steel substrate. This structural feature is consistent with effective surface coverage by the inhibitor layer. In addition, a minor $CaSO_4·2H_2O$ peak is detected, reflecting limited association of calcium species with sulfate ions in the corrosive medium.

Conclusion

The CaO/SiO_2 nanocomposite effectively inhibits corrosion of low-carbon steel in 15% HCl and 15% H_2SO_4 via adsorption and protective barrier-film formation. Electrochemical results (EIS) show improved charge-transfer resistance, while weight loss measurements verify a significant reduction in corrosion rate, consistent with the electrochemical behaviour. The inhibition efficiency depends on concentration and acidic medium, with optimum behaviour observed at 2 wt% in HCl and sustained improvement up to 10 wt% in H_2SO_4. SEM, EDX, and XRD analyses further support the development of a surface film that mitigates metal dissolution. Overall, the nanocomposite exhibits strong potential as an eco-friendly corrosion inhibitor for acidic environments.

Acknowledgement, The authors wish to express their sincere gratitude to the Tertiary Education Trust Fund, Nigeria (TETFund) and the Department of Chemistry, Akwa Ibom State University, for providing the enabling environment and support throughout the course of this research. Special thanks go to the Materials Chemistry Research Unit for access to laboratory facilities and technical assistance. We are also grateful to all colleagues who provided valuable insights and constructive feedback during the development of this manuscript. Finally, we acknowledge the contributions of our families for their encouragement and support.

Disclosure statement: *Conflict of Interest:* The authors declare that there are no conflicts of interest.
Compliance with Ethical Standards: This article does not contain any studies involving human or animal subjects.

References

AbdElRhiem, E., Khan, R., Ataya, S., & Abdelaziz, S. M. (2025). The hybrid protection method for copper alloy against electrochemical attack using benzotriazole and Sb_2O_3 nanoparticles synergy. *Scientific Reports*. 15, 43380, https://doi.org/10.1038/s41598-025-26605-w

Adamu, A. A., Iyun, O. R. A., & Habila, J. D. (2025). Adsorption and thermodynamic studies of the corrosion Inhibition effect of Desmodium adscendens (Swartz) extract on carbon steel in 2 M HCl. *BMC chemistry*, *19*(1), 163, https://doi.org/10.1186/s13065-025-01541-y

Akrout, H., Bousselmi, L., Maximovitch, S., Triki, E., & Dalard, F. (2012). Adsorption of corrosion inhibitors (SA, HEDP) using EQCM: chloride effect and synergic behavior. *Journal of materials science*, *47*(23), 8085-8093, DOI 10.1007/s10853-012-6702-x

Alao, A. O., Popoola, A. P., & Sanni, O. (2022). The influence of nanoparticle inhibitors on the corrosion protection of some industrial metals: A review. *Journal of Bio-and Tribo-Corrosion*, *8*(3), 68, https://doi.org/10.1007/s40735-022-00665-1

Aljibori, H. S., Alamiery, A., & Kadhum, A. A. H. (2023). Advances in corrosion protection coatings: A comprehensive review. *Int. J. Corros. Scale Inhib*, *12*(4), 1476-1520.

Anadebe, V. C., Harmayanti, A., Quadri, T. W., Elugoke, S. E., Thakur, A., Mathias, G. E., ... & Ebenso, E. E. (2026). Nanotechnology principles and nanomaterials in next-generation corrosion control: bridging sustainability with high-performance materials. *Advanced Composites and Hybrid Materials*. 9:229, https://doi.org/10.1007/s42114-026-01773-z

Assad, H., Lone, I. A., Sharma, P. K., & Kumar, A. (2025). Corrosion in the Oil and Gas Industry. *Industrial Corrosion: Fundamentals, Failure, Analysis and Prevention*, 39-63.

Avdeev, Y.G., Kuznetsov, Y.I. (2022). Acid corrosion of metals and its inhibition. A critical review of the current problem state. *International Journal of Corrosion and Scale Inhibition*, *11*(1), 111-141

Avdeev, Y. G., Nenasheva, T. A., Luchkin, A. Y., Marshakov, A. I., & Kuznetsov, Y. I. (2024). Effect of organic corrosion inhibitors on the kinetics of the cathodic hydrogen evolution reaction on steel in a sulfuric acid solution. *Russian Journal of Physical Chemistry B*, *18*(1), 111-124.

Azizian, S., Eris, S., & Wilson, L. D. (2018). Re-evaluation of the century-old Langmuir isotherm for modeling adsorption phenomena in solution. *Chemical physics*, *513*, 99-104.

Bhadeshia, H. K. D. H., & Honeycombe, R. W. K. (2024). *Steels: Structure, properties, and design*. Elsevier.

Boekom, E., Essien, K. E., Ekpo, V. F., & Obot, A. (2020). Kinetics, molecular dynamics and adsorption behaviour of pyridine on mild steel in 0.1 M HCl solution. *Elixir International Journal,* 142, 54382-54387.

Boekom, E., Essien, K., & Obot, A. (2019). Effects of thiophene on acid corrosion of mild steel. *World Journal of Applied Science and Technology,* 11(2), 174-180.

Borisova, D., Möhwald, H., & Shchukin, D. G. (2011). Mesoporous silica nanoparticles for active corrosion protection. *ACS nano*, *5*(3), 1939-1946.

Chaudhary, R., Kaur, A., Bala, N., Kansal, S. K., & Singh, S. (2026). Corrosion Resistance of Steel in Acidic Environments: A Comprehensive Review. *Journal of The Institution of Engineers (India): Series C*, 1-27.

Chen, L., Lu, D., & Zhang, Y. (2022). Organic compounds as corrosion inhibitors for carbon steel in HCl solution: a comprehensive review. *Materials*, *15*(6), 2023.

Chen, Y., Huang, H., Gao, Z., Liu, X., Wang, Q., Hou, L., & Wei, Y. (2025). Nanocontainers with synergistic inhibition for self-warning and self-repairing dual-functional coatings towards enhanced anticorrosion of Mg alloys. *Progress in Organic Coatings*, *208*, 109545, https://doi.org/10.1016/j.porgcoat.2025.109545

Cruz-Borbolla, J., Garcia-Ochoa, E., Narayanan, J., Maldonado-Rivas, P., Pandiyan, T., & Vásquez-Pérez, J. M. (2017). Electrochemical and theoretical studies of the interactions of a pyridyl-based corrosion inhibitor with iron clusters (Fe15, Fe30, Fe45, and Fe60). *Journal of molecular modeling*, *23*(12), 342,

Cunat, P. J. (2004). Alloying elements in stainless steel and other chromium-containing alloys. *Euro Inox*, *2004*, 1-24, https://doi.org/10.1007/s00894-017-3510-x

Essien, K. E., BoEkom, E. J., Okon, O. E., Odiongenyi, A. O., George, I., & Okon, E. J. (2023). Investigation of Corrosion Inhibition behaviour of 3-Methyl-5-Phenylisoxazole on Mild Steel Surface in HCl Solution. *J. Mater. Environ. Sci,* 14(7), 811-825.

Essien, K. E., Nelson, I. A., Obosi, E. J., Okon, E. J., & Umana, S. G. (2024b). Expired Glucored Forte drug: an eco-friendly corrosion inhibitor for mild steel. *Journal of Materials Science Research and Reviews,* 7(2), 302-314.

Essien, K. E., Odiongenyi, A. O., BoEkom, E. J., Abai, E. J., Eddy, N. O., Ekpenyong, O., & Okon, O. E. (2022). Corrosion inhibition potential of two isoxazole derivatives: experimental and Theoretical Analyses. *J. Mater. Environ. Sci,* 13(8), 928-944.

Essien, K. E., Okon, E. J., Archibong, I. N., Okon, O. E., & George, I. E. (2024a). Experimental, Quantum chemical and IR spectroscopy studies on the corrosion inhibition of mild steel by 3, 5-dimethyl-4-nitroisoxazole in HCl solutions. *J. Mater. Environ. Sci.,* 15 (1), 136, 150.

Essiene, K. E., Okon, O. E., Ekpenyong, I. O., & Effiong, J. O. (2021). Molecular Dynamics and Adsorption Behaviour of 2, 3-Diaminopyridine and 9, 10-Diaminophenanthrene In Neutral and Protonated Forms. *International Journal of Research and Innovation in Applied Science,* 6(5), 126-132.

Fekry, A. M., & Ameer, M. A. (2010). Corrosion inhibition of mild steel in acidic media using newly synthesized heterocyclic organic molecules. *International Journal of Hydrogen Energy*, *35*(14), 7641-7651, https://doi.org/10.1016/j.ijhydene.2010.04.111

Gaber, G. A., Hosny, S., & Heakal, F. E. T. (2025). Synthesis of copper schiff base nanocomplex as green inhibitor for 316 L stainless steel corrosion in an aggressive acidic environment. *Scientific Reports*, *15*(1), 36486.

Gao, W., Wang, S., Zhang, H., Wang, Q., Liu, H., Yu, H., & Dongbai, S. (2025). Low-cost application strategies of marine titanium alloys: titanium/steel dissimilar materials. *Metals*, *15*(11), 1205.

Gopal, K., Sunitha, D. V., & Prakash, A. G. (2026). PVP-driven surface engineered Ce 3+ doped Dy 2 O 3 nanoparticles for dual mode thermo and photoluminescence studies in TLD, forensic, anti-counterfeiting, and solid-state lighting applications. *Nanoscale*, *18*(11), 5831-5856.

Guendouz A., Ettahiri W., Adardour M., Lazrak J., El Assiri E.H., *et al.* (2025), New Benzimidazole Derivatives as Efficient Organic Inhibitors of mild steel Corrosion in Hydrochloric Acid Medium: Electrochemical, SEM/EDX, MC, and DFT Studies, *Journal of Molecular Structure,* 1321, 139901, ISSN 0022-2860, https://doi.org/10.1016/j.molstruc.2024.139901

Habibi, M., Joudaki, E., Moghadassi, A., & Moini Jazani, O. (2026). Enhancement of the Mechanical and Thermal Properties in Epoxy Film Adhesive Using APTES-Modified Zirconia Nanoparticles: Thermal Degradation Kinetics Study. *Polymer Composites*, *47*(11), 10241-10257.

Hasanin, M., & Al Kiey, S. A. (2023). Development of ecofriendly high performance anti-corrosive chitosan nanocomposite material for mild steel corrosion in acid medium. *Biomass Conversion and Biorefinery*, *13*(13), 12235-12248, https://doi.org/10.1007/s13399-021-02059-8

Hermas, A. E. A., Elnady, A. M., & Ali, R. M. (2019). Corrosion inhibition of stainless steel in sulfuric acid solution containing sulfide ions. *Anti-Corrosion Methods and Materials*, *66*(3), 360-368, https://doi.org/10.1108/ACMM-10-2018-2016

Hu, J., & Cheng, H. (2025). pH-responsive intelligent anticorrosion protection: catechol-driven organic–inorganic hybridization with TiO 2 and encapsulation by ZIF-90. *Journal of Materials Chemistry A*, *13*(45), 39436-39450.

Ituen, E., Akaranta, O., & James, A. (2017). Evaluation of performance of corrosion inhibitors using adsorption isotherm models: an overview. *Chem. Sci. Int. J*, *18*(1), 1-34.

Jackson, E., & Essien, K. E. (2019). Experimental and Theoretical Approach of L-Methionine Sulfone (LMS) as corrosion inhibitor for mild steel in HCL Solution. *Environment*, 1(2).

Jackson, E., Essien, K. E., & Okafor, P. C. (2016). Experimental and Quantum Studies: A New Corrosion Inhibitor for Mild Steel. *Elixir Corrosion and Dye*, 86, 34978-34983.

Jiang, J., & Liu, J. (2022). Iron anode-based aqueous electrochemical energy storage devices: recent advances and future perspectives. *Interdisciplinary Materials*, *1*(1), 116-139.

Kania, H. (2023). Corrosion and anticorrosion of alloys/metals: the important global issue. *Coatings*, *13*(2), 216.

Koch, G. H., Brongers, M. P., Thompson, N. G., Virmani, Y. P., & Payer, J. H. (2005). Cost of corrosion in the United States. In *Handbook of environmental degradation of materials* (pp. 3-24). William Andrew Publishing.

Kolics, A., & Wieckowski, A. (2001). Adsorption of bisulfate and sulfate anions on a Pt (111) electrode. *The Journal of Physical Chemistry B*, *105*(13), 2588-2595.

Kufre, E. E., Akanimo, N. E., & Aniedi, E. N. (2025). Emerging Role of Calcium Oxide Nanoparticles in the Photocatalytic Breakdown of Organic Contaminants from Industrial Effluents. *J. Mater. Environ. Sci.,* 16 (9), 1668, 1683.

Lame, A., Farruku, M., Kokalari, E., Xhanari, K., Isak, N., Xhaxhiu, K., Shehu, A. (2024). Walnut (Juglans regia L.) fruit septum alcoholic extract as corrosion inhibitor for Fe B500B steel bars in mixed acidic solution. *Journal of Electrochemical Science and Engineering*, *14*(3), 297-320.

Liu, G., Li, J., & Zhang, Y. (2024). Corrosion of carbon steels subjected to chloride and sulfate in simulated concrete pore solutions with different pH. *Construction and Building Materials*, *440*, 137445.

Liu, X., & Lee, D. J. (2014). Thermodynamic parameters for adsorption equilibrium of heavy metals and dyes from wastewaters. *Bioresource technology*, *160*, 24-31.

Lrhoul H., Sekkal H., Hammouti B. (2023) Natural Plants as Corrosion Inhibitors: Thermodynamic's restrictions, *Mor. J. Chem.,*14(3), 689-698, https://doi.org/10.48317/IMIST.PRSM/morjchem-v11i3.40144

Mu'azu, K., Aliyu, M. M., Mohammed, A. T., Lasisi, S., Dahiru, R., & Suleiman, I. Y. (2022). Ethanol extract of avocado leaf as corrosion inhibitor for the protection of mild steel in acidic environment. *J. Mater. Environ. Sci*, *13*(11), 1343-1354.

Muresan, L. M. (2023). Nanocomposite coatings for anti-corrosion properties of metallic substrates. *Materials*, *16*(14), 5092.

Numin, M. S., Pathirana, M., Jumbri, K., Varela, B., Kee, K. E., & Tan, M. Y. (2026). Discovering synergistic localised corrosion inhibitors through local polarisation measurements using electrode arrays. *Corrosion Science*, 113978, https://doi.org/10.1016/j.corsci.2026.113978

Obot, A. S., BoEkom, E. J., Ituen, E. B., Ugi, B. U., Essien, K. E., & Jonah, N. B. (2021). Thermodynamic investigation and quantum chemical evaluation of n-hexane extracts of Costus lucanusianus as corrosion inhibitors for mild steel and aluminum in 1 M HCl solution. *J. Appl. Phys. Sci. Int*, 13, 6-27.

Oguzie, E.E., Oguzie, K.L., Akalezi, C.O., Udeze, I.O., Ogbulie, J.N., Njoku, V.O. (2013). Natural products for materials protection: Corrosion and microbial growth inhibition using Capsicum frutescens biomass extracts. *ACS Sustainable Chemistry & Engineering*, *1*(2), 214-225.

Okolo, D. C., Tom-Okoro, M. E., Anumudu, J., Nwadirichi, B. U., & Ndukwe, A. I. (2026). Green corrosion inhibitors-A sustainable approach to metal protection in aggressive environment. *Zastita Materijala*.

Okon, K., Ekeke, I.C., Maduabuchi, C.A., Ayogu, I.I., Taofik, O.A., Akalezi, C.O. (2025). Recent advances in the use of metal oxides as corrosion inhibitors: a review. *Koroze a Ochrana Materiálu*, *69*(1), 14-33.

Oreko, B. U., & Okuma, S. O. (2025). Recent advances in nanoparticle-based corrosion inhibition of metals: A review. *NIPES-Journal of Science and Technology Research*, *7*(3), 245-265, https://doi.org/10.37933/nipes/7.3.2025.1449

Oueslati, K., Nasti, R., Magni, M., Trasatti, S., Amor, Y.B. (2025). Glaucium Extract as an Effective Green Corrosion Inhibitor for a Mild Steel in High Concentrated Sulfuric Acid Solution. *ChemistrySelect*, *10*(21), e00514, https://doi.org/10.1002/slct.202500514

Ozoemena, C.P., Boekom, E.J., Abai, E.J., Edet, E.K., Akpan, I.A. (2023). Schiff Base and Its Metal Complexes as Ecofriendly Pitting Corrosion Inhibitors on ASTM-A3 6 Low Carbon Steel in Corrosive Oil and Gas Well Treatment Fluids. *Science Journal of Chemistry*, 11(5), 168-188.

Ozoemena, C. P., Boekom, E. J., Akpan, G. J., Asuquo, I. G., Edet, E. K., & Jacob, A. E. (2024). Computational Modelling and Comparative Analysis of a Schiff Base Ligand and Its Analog as Inhibitors Against Mild Steel Corrosion in 1M HCl. *Journal of Sustainable Materials Processing and Management*, 4(1), 71-88.

Pradityana, A., Setiawan, E., Khosfirah, F., Nik, W. M. N. W., & Izionworu, V. O. (2026). Adsorption-controlled corrosion protection of mild steel in acidic environment using Xanthosoma undipes leaf extract: An integrated electrochemical and SEM analysis. *South African Journal of Chemical Engineering*, 100882.

Prasad, A. R., Kunyankandy, A., & Joseph, A. (2020). Corrosion inhibition in oil and gas industry: Economic considerations. *Corrosion inhibitors in the oil and gas industry*, 135-150.

Răuță, D. I., Matei, E., & Avramescu, S. M. (2025). Recent development of corrosion inhibitors: types, mechanisms, electrochemical behavior, efficiency, and environmental impact. *Technologies*, *13*(3), 103.

Revie, R. W., & Uhlig, H. H. (2025). *Corrosion and corrosion control*. John Wiley & Sons.

Rios, J. F., Calderón, J. A., & Nogueira, R. P. (2013). Electrochemical behavior of metals used in drinking water distribution systems: a rotating cylinder electrode's study. *Corrosion*, *69*(9), 875-885.

Saha, S. K., Dutta, A., Ghosh, P., Sukul, D., Banerjee, P. (2015). Adsorption and corrosion inhibition effect of Schiff base molecules on the mild steel surface in 1 M HCl medium: a combined experimental and theoretical approach. *Physical Chemistry Chemical Physics*, *17*(8), 5679-5690.

Sahmoune, M. N. (2019). Evaluation of thermodynamic parameters for adsorption of heavy metals by green adsorbents. *Environmental Chemistry Letters*, *17*(2), 697-704.
Sasikumar, Y., Kumar, A. M., Gasem, Z. M., & Ebenso, E. E. (2015). Hybrid nanocomposite from aniline and CeO2 nanoparticles: Surface protective performance on mild steel in acidic environment. *Applied Surface Science*, *330*, 207-215, 10.1016/j.apsusc.2015.01.002
Selvi, J.A., Arthanareeswari, M., Pushpamalini, T., Rajendran S., Vignesh T. (2020). Effectiveness of Vinca rosea leaf extract as corrosion inhibitor for mild steel in 1 N HCl medium investigated by adsorption and electrochemical studies. *Int. J. Corros. Scale Inhib*, *9*(4), 1429-1443.
Solmaz, R., Mert, M. E., Kardaş, G., Yazici, B., & Erbil, M. E. H. M. E. T. (2008). Adsorption and corrosion inhibition effect of 1, 1′-thiocarbonyldiimidazole on mild steel in H2SO4 solution and synergistic effect of iodide ion. *Acta Physico-Chimica Sinica*, *24*(7), 1185-1191, https://doi.org/10.1016/S1872-1508(08)60053-4
Stefanoni, M., Angst U., Elsener B. (2015). Local electrochemistry of reinforcement steel–distribution of open circuit and pitting potentials on steels with different surface condition. *Corrosion Science*, *98*, 610-618.
Thakur, A., Kaya, S., & Kumar, A. (2023). Recent trends in the characterization and application progress of nano-modified coatings in corrosion mitigation of metals and alloys. *Applied Sciences,* 13(2), 730, https://doi.org/10.3390/app13020730
Vakili, M., Koutník, P., Kohout, J., & Gholami, Z. (2024). Analysis, assessment, and mitigation of stress corrosion cracking in austenitic stainless steels in the oil and gas sector: a review. *Surfaces*, 7(3), 589-642.
Wang, X., Ma, X. Z., Yang, J. C., Chen, T., Shi, L., Zhang, X. X., & Dong, Z. H. (2026). Unravelling lubrication and tribo-corrosion inhibition mechanisms of surface-active ionic liquids on carbon steel: Tribo-electrochemistry and theoretical analysis. *Corrosion Science,* 113706.
Yang, J., Hou, D., & Ding, Q. (2018). Ionic hydration structure, dynamics and adsorption mechanism of sulfate and sodium ions in the surface of calcium silicate hydrate gel: A molecular dynamics study. Applied Surface Science, 448, 559-570.
Zamindar, S., Mandal, S., Murmu, M., & Banerjee, P. (2024). Unveiling the future of steel corrosion inhibition: a revolutionary sustainable odyssey with a special emphasis on N+-containing ionic liquids through cutting-edge innovations. *Materials Advances*, 5(11), 4563-4600, DOI: 10.1039/d4ma00156g
Zarrok H., Oudda H., El Midaoui A., Zarrouk A., Hammouti B., Ebn Touhami M., Attayibat A., Radi S., Touzani R. (2012) Some New Bipyrazole Derivatives as Corrosion Inhibitors for C38 Steel in Acidic Medium, *Res. Chem. Interm.,* 38 N°8, 2051-2063, DOI 10.1007/s11164-012-0525-x
Zarrouk A., Messali M., Zarrok H., Salghi R., Al-Sheikh Ali A., B. Hammouti, Al-Deyab S.S., Bentiss F. (2012), Synthesis, Characterization and Comparative Study of New Functionalized Imidazolium-Based Ionic Liquids Derivatives Towards Corrosion of C38 Steel in Molar Hydrochloric Acid, *Int. J. Electrochem. Sci.,* 7(8), 6998-7015.
Zehra, S., Aslam, R., Mobin, M., & Verma, C. (Eds.). (2025). Industrial Corrosion: Fundamentals, Failure, Analysis and Prevention. John Wiley & Sons.